ECS Transactions, 68 (1) 3333-3343 (2015)
10.1149/06801.3333ecst ©The Electrochemical Society

# Water Splitting on Model-Composite $La_{0.6}Sr_{0.4}FeO_{3-\delta}$ (LSF) Electrodes in $H_2/H_2O$ Atmosphere

A. K. Opitz[a], A. Nenning[a], S. Kogler[a], C. Rameshan[b], R. Rameshan[c,d], R. Blume[d,e], M. Hävecker[d,e], A. Knop-Gericke[d], G. Rupprechter[b], B. Klötzer[c], J. Fleig[a]

[a] Vienna University of Technology, Institute of Chemical Technologies and Analytics, Getreidemarkt 9/164-EC, 1060 Vienna, Austria
[b] Vienna University of Technology, Institute of Materials Chemistry, Getreidemarkt 9/165-PC, 1060 Vienna, Austria
[c] University of Innsbruck, Institute of Physical Chemistry, Innrain 80-82, 6020 Innsbruck, Austria
[d] Fritz Haber Institute of the Max Planck Society, Department of Inorganic Chemistry, Faradayweg 4–6, 14195 Berlin, Germany
[e] Catalysis for Energy, Group E-GKAT, Helmholtz-Zentrum Berlin fuer Materialien und Energie GmbH, Division Solar Energy Research, Elektronenspeicherring BESSY II, Albert-Einstein-Strasse 15, 12489 Berlin, Germany

Mixed conducting cathodes for solid oxide electrolysis cells (SOECs) offer a promising alternative to the nowadays used Ni/YSZ cermet. Here, the water splitting kinetics of mixed conducting perovskite-type $La_{0.6}Sr_{0.4}FeO_{3-\delta}$ (LSF) thin film electrodes was investigated in humid reducing atmospheres at 600 – 650 °C. Under equilibrium conditions an area specific surface resistance of ca. 15 Ωcm² was obtained on freshly prepared electrodes. Upon cathodic polarization of more than 20 mV a strong decrease of the surface resistance was observed. This acceleration of the water splitting kinetics was accompanied by the formation of metallic iron particles on the LSF surface, which was observed by means of near-ambient pressure XPS experiments.

## Introduction

Water electrolysis is a possible approach for chemical storage of excess electrical energy from sustainable sources such as solar and wind energy. In this respect, solid oxide electrolysis cells (SOECs) are highly promising owing to their very high efficiencies. Currently, research activities on SOECs are often based on standard solid oxide fuel cells (SOFCs) operating in reverse mode (1-3). Thus, the cathode of these SOECs consists of a common Ni/yttria-stabilized zirconia (YSZ) composite electrode. Since the reverse overpotential at the Ni/YSZ electrode during SOEC operation causes different electrode performance and higher degradation rates than under SOFC conditions (2, 4) electrode optimization is one of the main objectives in current SOEC research.

An approach to improve SOECs is to replace the Ni/YSZ cermet by mixed conducting cathodes and acceptor doped perovskite-type materials are possible candidates. Owing to its stability under (wet) reducing conditions and its well-known defect chemistry (5), $La_{0.6}Sr_{0.4}FeO_{3-\delta}$ (LSF) is an excellent model material for the investigation of mixed conducting SOEC cathodes. A disadvantage of acceptor doped

oxides (and therefore also LSF) under reducing conditions is their rather low electronic conductivity (6). In case of thin film electrodes, this poor electronic charge transport can cause an electronic sheet resistance and may thus lead to inhomogeneous electrochemical polarization (7, 8). However, by applying metallic thin film current collectors (9, 10) the electrochemical surface activity of large parts of mixed conducting electrodes can be exploited and the corresponding surface properties can be separated from resistances due to poor current distribution.

In the present study, the electrochemical surface activity of LSF thin film electrodes under $H_2/H_2O$ atmosphere is investigated by means of impedance spectroscopy and electrochemical dc methods. To ensure a homogeneous electrochemical polarization and to allow for a separation of surface resistance and electronic current transport within the thin film electrode, Pt current collectors were deposited at the electrode/electrolyte interface. For the sake of comparison, these LSF model-composite electrodes were also characterized under oxidizing conditions. Substantial changes of the surface properties of LSF upon cathodic polarization are furthermore investigated by in-situ near ambient pressure XPS.

## Experimental

Sample Preparation

LSF thin films were prepared by pulsed laser deposition. The target was prepared from $La_{0.6}Sr_{0.4}FeO_{3-\delta}$ powder (Sigma-Aldrich) by cold isostatic pressing and sintering (1250°C, 5 h, air). Ablation of the target was performed by a 248 nm KrF excimer laser (Lambda COMPexPro 201F) in an atmosphere of $4\times10^{-2}$ mbar pure oxygen with a laser pulse repetition rate of 5 Hz and a nominal laser pulse energy of 400 mJ. As substrate single crystalline (100)-oriented YSZ electrolyte (Crystec, Germany) was used. The substrate temperature during deposition was 650 °C, which was measured by a pyrometer (Heitronics, Germany). Deposition times were adjusted such that film thicknesses of 200 ± 20 nm were obtained. Prior to the PLD process a current collecting thin film grid was prepared on the YSZ substrate by sputter deposition of 10 nm Ti and 100 nm Pt, followed by a photolithographical micro-patterning process and Ar-ion beam etching.

For electrochemical characterization, circular microelectrodes with diameters of 50, 100, and 200 µm were prepared from the model-composite thin films (LSF on current collecting grid) by a further photolithographic and Ar-ion beam etching step. A sketch and a scanning electron microscopy (SEM) image of the model-composite electrodes are depicted in Fig. 1. For near-ambient pressure XPS (NAP-XPS) measurements, macroscopic LSF thin film electrodes with Pt grid beneath (0.111 cm² active area) were used. On the bottom side of both types of samples porous paste LSF/Pt counter electrodes (CE) were deposited – details of the counter electrode preparation are given in the supporting information of Ref. (11). The polarization resistance of the counter electrode at 620°C in an atmosphere of ~2.5% $H_2$/~2.5% $H_2O$/balance Ar was about 8 Ω. This is significantly smaller than the polarization resistance of both the microscopic and the macroscopic thin film working electrodes (see below) and thus the electrochemical reversibility of the counter electrodes can safely be assumed. A sketch of the samples used for the in-situ XPS experiments is shown in Fig. 2.

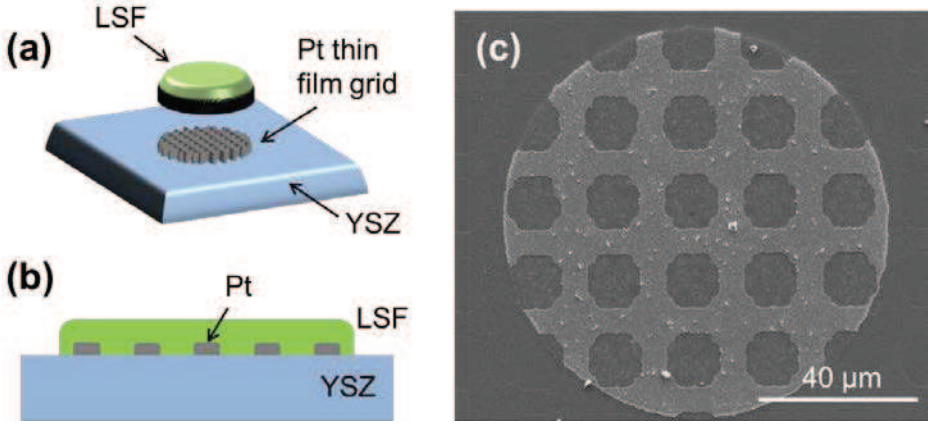


Figure 1. Sketch of a model-composite microelectrode with buried Pt current collector: (a) Oblique view with LSF artificially lifted to make the current collector visible. (b) Cross-section. (c) SEM image of an LSF microelectrode with buried Pt current collecting grid.

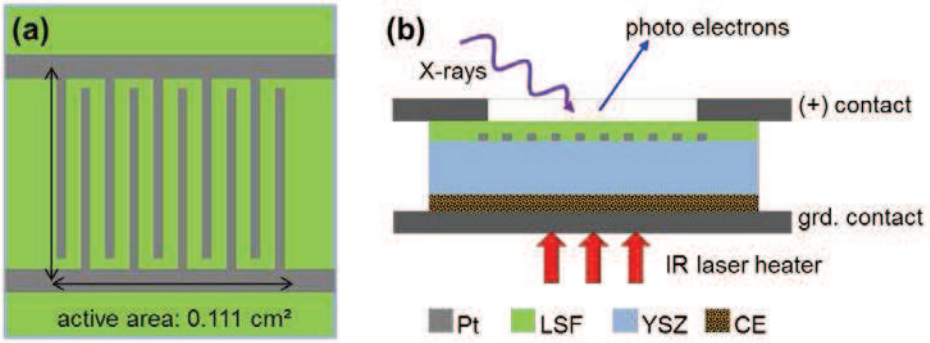


Figure 2. Sketch of the macroscopic samples used for in-situ XPS measurements: (a) Top view of the LSF working electrode. (b) Cross-section of the sample mounted in the NAP-XPS setup.

Electrochemical Experiments

Electrochemical characterization of the model-composite electrodes was carried out by impedance spectroscopy measurements (Novocontrol Alpha-A high performance frequency analyzer equipped with a POT/GAL 30V 2A interface) in a homebuilt micro-contact setup. It allows contacting of individual microelectrodes by Pt/Ir tips, heating of the sample up to 1000°C and control of the atmosphere – in the present experiments the atmosphere was ~2.5% $H_2$/~2.5% $H_2O$/balance Ar or synthetic air. The electrode temperature was calculated from the spreading resistance of ion conduction in the YSZ electrolyte (see below) and was about 610 – 620°C. Further details regarding the micro-contact setup and the procedure of calculating true electrode temperatures are given in Refs. (12, 13).

Simultaneous Electrochemical and In-Situ XPS Measurements

The NAP-XPS measurements with simultaneous electrochemical experiments were performed at the ISISS beam line of synchrotron HZB/BESSY II in Berlin (14, 15). The

main parts of the NAP-XPS setup are a high pressure cell, which allows measurements at pressures up to 20 mbar, and an attached differentially pumped hemispherical analyzer (Phoibos 150 Plus, SPECS) including a 2D delay line detector. For a more detailed description of the NAP-XPS setup the reader is referred to Refs. (16, 17).

For the simultaneous XPS and electrochemical measurements the samples with the macroscopic LSF model-composite electrodes were mounted between two platinum sheets which were both mechanical fixation and electrical contacting of the two electrodes (working electrode: +, counter electrode: grounded). The Pt sheet contacting the working electrode offered a hole for the XPS measurements and the Pt back sheet was also used for heating of the samples by means of an infrared laser (see Fig. 2b). The sample temperature was measured by a pyrometer as well as by the conductivity of the YSZ electrolyte obtained from electrochemical impedance measurements (12). Both methods yielded temperatures of 620 ± 15°C. In the experimental chamber the pressures of both $H_2$ and $H_2O$ were set to 0.25 mbar, yielding a total pressure of 0.5 mbar.

Impedance spectroscopy measurements (Novocontrol Alpha-A high performance frequency analyzer with POT/GAL 30V 2A interface) were conducted at frequencies between 10 mHz and 1 MHz and the ac voltage was limited to 5 mV rms to avoid XPS peak broadening. Electrochemical polarization was achieved by applying dc voltages between +700 mV and -500 mV to the working electrode and at each set voltage XPS data was recorded after reaching a steady state dc current. In these experiments La3d, Sr3d, Fe2p, and O1s spectra were recorded. In the present study, however, only the Fe2p spectra measured at 845 eV photon energy with an approximate information depth of 0.5 nm are discussed. Interpretation of the other data will be given in a forthcoming paper.

## Results and Discussion

### Impedance Spectroscopy under Equilibrium Conditions

An impedance spectrum measured on a freshly prepared 200 µm sized circular LSF microelectrode with buried Pt current collector in $H_2/H_2O$ is shown in Fig. 3a. It consists of three well separated features: (i) A high frequency intercept, which can be attributed to the spreading resistance of ion conduction in YSZ (18). (This resistance was also employed for calculation of true electrode temperatures – for details please refer to Ref. (12).) (ii) A medium frequency arc most likely related to processes at the electrode/electrolyte interface, and (iii) a low frequency semicircle. The diameter of the latter one corresponds to the oxygen exchange resistance at the surface of the electrode (i.e. of the reaction $H_2 + O^{2-} \rightleftharpoons H_2O + 2\,e^-$) (18). Since no additional feature was observed originating from electronic charge transport within the LSF thin film, the mesh width of the buried Pt current collector is sufficiently small and thus homogeneous polarization of the electrode can safely be assumed. The oxygen exchange resistance at the surface of the LSF electrodes was estimated by fitting the spectra to the simplified equivalent circuit shown in Fig. 3d. In this circuit the element $R_{surface}$ represents the surface resistance of LSF (10, 19), the constant phase element CPE and the serial resistor $R_{offset}$ are used to yield sufficient fit quality and are not further considered in this study. From the surface resistance and the size of the electrode an area specific resistance of about 15 Ωcm² can thus be obtained.

For the sake of comparison, also measurements in synthetic air were conducted on the model-composite electrodes – a resulting impedance spectrum is depicted in Figs. 3b and 3c. Its features are qualitatively very similar to the spectrum obtained in reducing atmosphere. The main difference is the larger low frequency arc (as well as a somewhat larger chemical capacitance – compare relaxation frequencies in Fig. 3a and 3b). For obtaining an area specific resistance, however, one has to take into account that here the part of the LSF surface above the current collecting Pt grid is not electrochemically active owing to the low ionic conductivity and thus large ionic in-plane resistance of LSF in air. For details regarding electrochemically active surfaces of mixed conducting model-composite electrodes in dependence of the oxygen partial pressure the reader is referred to Ref. (10). Considering this reduced active area in air an area specific surface resistance of ca. 16 Ωcm² can be calculated. Since the inverse polarization resistances are a direct measure for the electrochemical oxygen exchange rates at the electrode surfaces, the activity of the LSF surface for oxygen reduction and water splitting can be concluded to be rather similar at the present temperature. Moreover, this result suggests that an application of LSF as an SOEC cathode may lead to polarization resistances comparable to that of nowadays used porous paste SOFC cathodes. (Please note that the given polarization resistances are normalized to the true active surface area and much smaller values are thus possible for porous electrodes.) This potential applicability makes the behavior of LSF electrodes in $H_2/H_2O$ atmospheres under cathodic polarization a highly interesting topic.

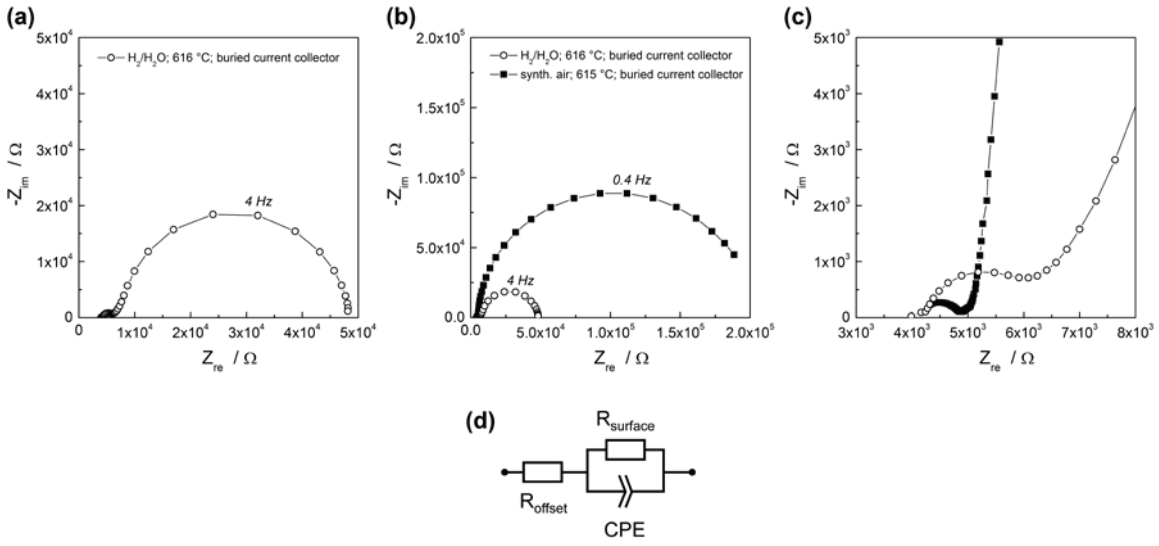


Figure 3. Impedance spectra measured on 200 µm LSF/Pt model-composite electrodes at ca. 615°C. (a) Measurement in $H_2/H_2O$ atmosphere. (b) Comparison of measurements in $H_2/H_2O$ atmosphere and in synthetic air. (c) Magnification of the high frequency part of the spectra in (b). (d) Equivalent circuit used for data analysis.

Impedance Spectroscopy under Electrochemical Polarization

In Fig. 4 impedance spectra are shown measured under different electrochemical bias load. These spectra were recorded on macroscopic samples during in-situ NAP-XPS measurements. Qualitatively the spectra are comparable to those in Fig. 3. However, the area specific resistance is significantly higher than above. This can be attributed to degradation effects occurring in the samples pre-history since these measurements were not recorded on freshly prepared samples (unlike those in Fig. 3). Rather, a number of

experiments were already conducted on this sample and LSF thin films are known to be prone to degradation, e.g. upon gas changes between oxidizing and reducing conditions (19).

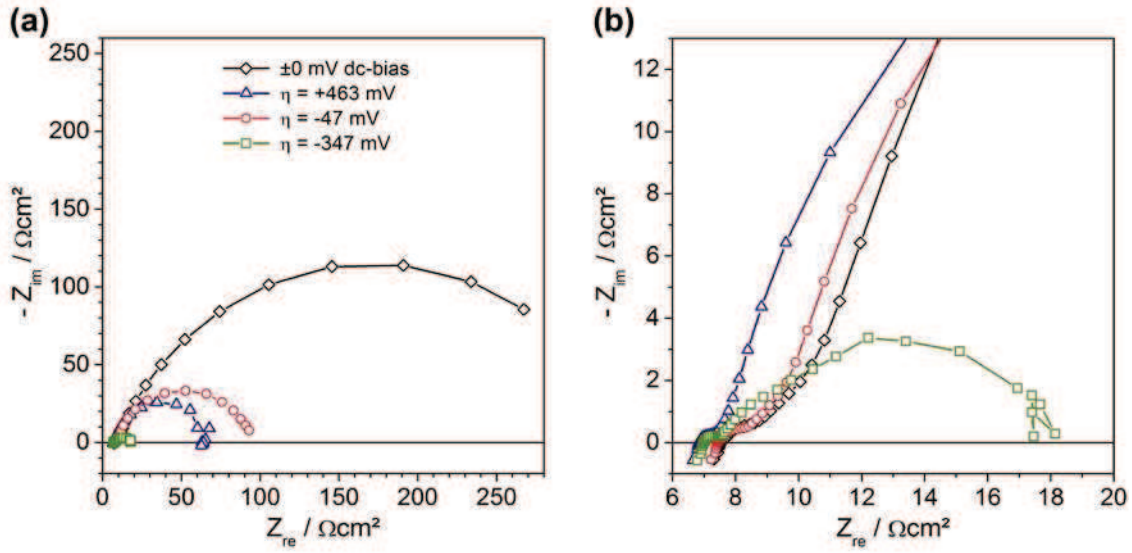


Figure 4. (a) Impedance spectra measured on macroscopic LSF samples simultaneously to NAP-XPS experiments under different electrochemical polarization. (b) Magnification of the high frequency regime of (a).

Nevertheless, a comparison of the differently polarized impedance spectra in Fig. 4 is still possible since they were measured within relatively short times and without any other experiments in between. Hence, large degradation effects during the measurements can be ruled out. It can be seen that the low frequency arc attributed to the electrochemical reaction at the LSF surface is decreased by anodic as well as by cathodic polarization. Such a decrease is a usual characteristic of non-linear resistances such as electrochemical surface resistances. Rather uncommon, however, is the very asymmetric behavior of the electrode impedance upon polarization: An anodic overpotential of +463 mV leads to a decrease of the surface resistance by a factor of about five. Approximately the same decrease can be achieved by applying a cathodic overpotential of only –47 mV and a high cathodic polarization of $\eta = -347$ mV leads to a decrease of the differential surface resistance by a factor of about 25.

Quantitative analysis of the surface resistance was done by the same procedure as already described – the measured spectra were fitted to the equivalent circuit in Fig. 3d. The surface resistance was related to the active area of the LSF working electrode (0.111 cm²). A plot of the resulting area specific resistance versus the applied overpotential is shown in Fig. 5a. From this diagram the strongly asymmetric electrode kinetics becomes even more obvious. For cathodic polarizations of more than ca. –20 mV a strong decrease of the surface resistance can be observed. This step-like change in electrode kinetics is rather uncommon and indicates a strong increase in the activity of LSF for the water splitting reaction by a change of the reaction mechanism.

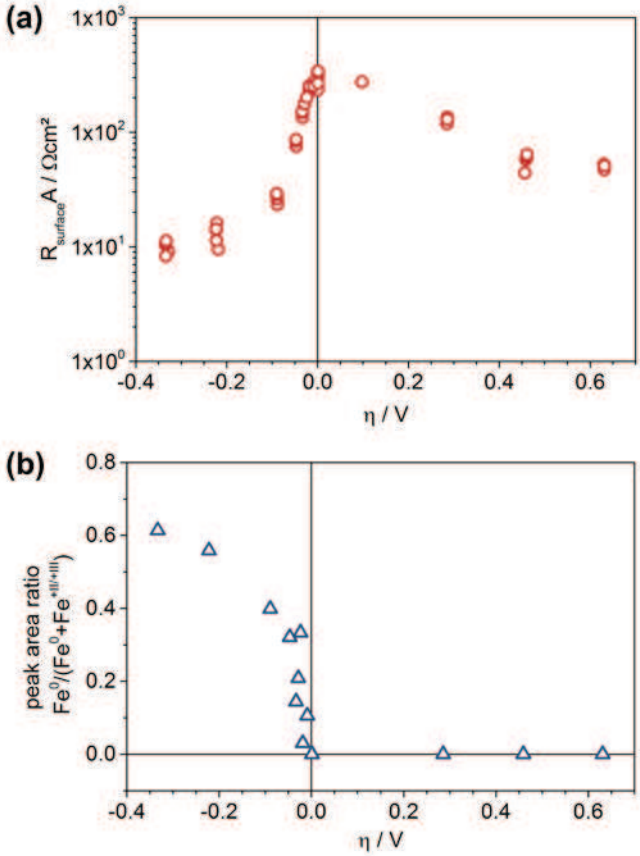


Figure 5. (a) Area related differential surface resistances from bias-dependent impedance measurements plotted as a function of the applied overpotential. Simultaneously NAP-XPS experiments were performed. (b) $Fe2p_{3/2}$ peak area fraction of metallic iron (with respect to the total peak area of iron) plotted versus the applied overpotential.

NAP-XPS Measurements – Fe2p Spectra

Fe2p XPS measured at 845 eV incident beam energy are depicted in Fig. 6a and depending on the simultaneously applied overpotential two significantly different types of spectra can be observed: (i) Without voltage load and under anodic polarization only two pronounced peaks at binding energies (BE) of ~710 eV and ~724 eV are obvious. Both features can be attributed to $Fe2p_{3/2}$ and $Fe2p_{1/2}$, respectively, and the measured BE values are in reasonable agreement with literature values of $Fe^{+II}$ and/or $Fe^{+III}$ (20). For separation of $Fe^{+II}$ and $Fe^{+III}$, an analysis of $Fe2p_{3/2}$ satellites would be necessary, which, however, is not the main goal of the present paper. Thus, in the following $Fe^{+II}$ and $Fe^{+III}$ species are jointly referred to as "oxidized species".

(ii) At cathodic overpotentials higher than ca. –20 mV two further XPS peaks at about 707 eV and 720 eV were observed, which can be attributed to $Fe2p_{3/2}$ and $Fe2p_{1/2}$ of metallic iron, respectively. It should be emphasized that the electrode did not irreversibly decompose upon formation of the metallic Fe species. Rather, the cathodically evolved $Fe^0$ was quickly re-oxidized after retracting the applied voltage. Exsolution of transition metal particles from perovskite type electrodes under reducing conditions was already reported in literature (21, 22). There, also a highly reversible behavior of exsolution and re-integration of the respective metal was described. The results presented in these studies, together with the fact that LSF is already close to its

stability limit and the observation that upon metallic iron formation a Fermi-edge was found in the valence band spectra (not shown), makes the formation of metallic iron particles on the LSF surface the most likely interpretation for the observed changes in the Fe2p XPS spectra.

Deconvolution of Fe2p spectra was done by means of the software CasaXPS using a simplified peak model based on a line-shape related to the asymmetric Lorentian – for further details regarding the fitting of XPS spectra please refer to Ref. (11). Since the main objective was quantification of the relative proportions of metallic and oxidic iron, only the $Fe2p_{3/2}$ peak was used for further analysis. In Fig. 6b the fits of the $Fe2p_{3/2}$ feature for strongly cathodic and strongly anodic polarization of two different measurements are compared with the measurement data. From these fits peak area values were extracted, which are used in the following discussion.

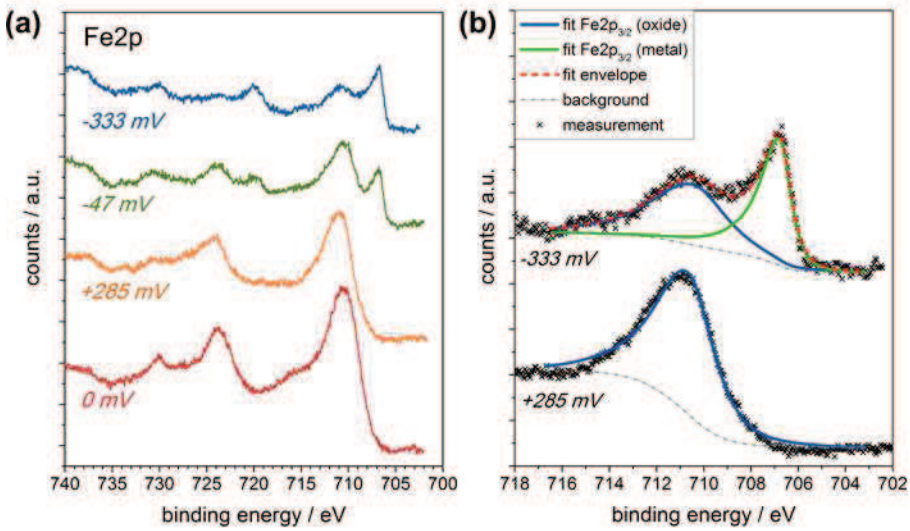


Figure 6. (a) Fe2p XPS spectra measured with a photon energy of 845 eV under simultaneous electrochemical polarization. The applied overpotentials are indicated for each spectrum. (b) Comparison of measurement and fit result of the $Fe2p_{3/2}$ features of a strongly cathodically and a strongly anodically polarized LSF electrode.

Relation of $Fe^0$ Evolution and Electrochemical Performance Increase

The fraction of the $Fe^0$ peak area with respect to the sum of $Fe^0$ and $Fe^{+II/+III}$ peak areas is plotted as a function of the applied overpotential in Fig. 5b. The metallic iron species suddenly appears for cathodic voltages more negative than ca. –20 mV. By comparing Fig. 5a and 5b it becomes obvious that the above mentioned increase of the electrode's water splitting activity is accompanied by the formation of a metallic iron species at the surface of the electrode. In Fig. 7 a logarithmic plot of the inverse area specific resistance under cathodic polarization versus the fraction of metallic iron is shown. The diagram suggests a strong dependence of the water splitting activity of LSF on the amount of metallic iron at the surface of the electrode.

An unambiguous mechanistic interpretation, however, is not possible from the data available so far. On the one hand, the accelerated water splitting kinetics at cathodic polarization may be due to a catalytic effect of the metallic iron particles on the LSF

surface. On the other hand also the remaining iron-depleted LSF surface may offer fast kinetics for the water splitting reaction. Nevertheless, the observed correlation of metal exsolution and electrochemical performance increase suggests a fundamentally different water splitting mechanism in presence of the metallic iron species and may provide new possibilities in the search for optimized SOEC cathodes for high-temperature electrochemical water splitting.

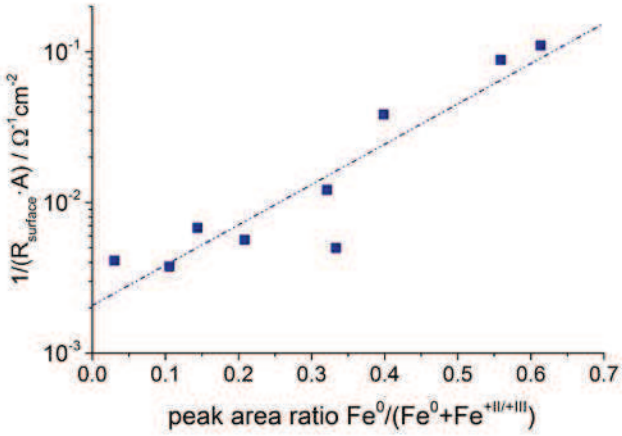


Figure 7. Logarithmic plot of the inverse area-related surface resistance of cathodically polarized LSF electrodes versus the peak area fraction of metallic iron. The line represents a guide to the eye.

## Conclusions

The electrochemical activity of mixed conducting LSF electrodes for the water splitting reaction was studied by impedance spectroscopy. To compensate for the relatively low electronic conductivity of LSF under reducing conditions a sputter deposited Pt current collector was buried beneath the LSF film. Interestingly, the surface resistance of these model-composite electrodes (which is a measure of the electrochemical surface activity) at ca. 610°C in $H_2/H_2O$ atmosphere was very similar to the surface resistance in synthetic air. The value of ca. 15 $\Omega cm^2$ (with respect to the true area) obtained on freshly prepared electrodes suggests a quite high water splitting activity of LSF.

In the second part of the study NAP-XPS investigations of electrochemically polarized LSF electrodes were performed simultaneously to impedance spectroscopy measurements. In these in-situ experiments, which were carried out at synchrotron BESSY II in Berlin, the evolution of metallic iron was observed under cathodic polarization more negative than –20 mV. The exsolution of $Fe^0$ was accompanied by an almost step-like decrease of the surface resistance of LSF leading to a highly asymmetric current–voltage curve. This rather uncommon behavior strongly indicates a mechanistic change of the water splitting kinetics at the LSF surface, when metallic iron is present.

## Acknowledgements

This work was financially supported by the Austrian Science Fund (FWF) through grants F4502/03/09 (SFB FOXSI) and W1243. We acknowledge the Helmholtz-Zentrum

Berlin for provision of synchrotron radiation beamtime at beamline ISIS-PGM of BESSY II and would like to thank the BESSYstaff for assistance. Moreover, the research leading to these results has received funding from the European Community's Seventh Framework Programme (FP7/2007-2013) under grant agreement number 226716. Finally we thank Dr. Dmitry Zemlyanov for helpful discussions and Elisabeth Eitenberger for her kind assistance during the SEM measurements.

## References

1. J. E. O'Brien, J. J. Hartvigsen, S. Elangovan, C. M. Stoots, J. S. Herring and P. A. Lessing, *Journal of Fuel Cell Science and Technology*, **2**, 156 (2005).
2. A. Hauch, S. D. Ebbesen, S. H. Jensen and M. Mogensen, *J. Electrochem. Soc.*, **155**, B1184 (2008).
3. J. S. Herring, J. E. O'Brien, C. M. Stoots, G. L. Hawkes, J. J. Hartvigsen and M. Shahnam, *Int. J. Hydrogen Energy*, **32**, 440 (2007).
4. T. Matsui, R. Kishida, J.-Y. Kim, H. Muroyama and K. Eguchi, *J. Electrochem. Soc.*, **157**, B776 (2010).
5. M. Kuhn, S. Hashimoto, K. Sato, K. Yashiro and J. Mizusaki, *Solid State Ionics*, **195**, 7 (2011).
6. M. V. Patrakeev, J. A. Bahteeva, E. B. Mitberg, I. A. Leonidov, V. L. Kozhevnikov and K. R. Poeppelmeier, *Journal of Solid State Chemistry*, **172**, 219 (2003).
7. A. Wedig, M. E. Lynch, R. Merkle, J. Maier and M. Liu, *ECS Transactions*, **45**, 213 (2012).
8. A. K. Opitz, M. Kubicek, S. Huber, T. Huber, G. Holzlechner, H. Hutter and J. Fleig, *J. Mater. Res.*, **28**, 2085 (2013).
9. W. C. Chueh, Y. Hao, W. Jung and S. M. Haile, *Nature Materials*, **11**, 155 (2012).
10. A. Nenning, A. K. Opitz, T. Huber and J. Fleig, *Phys. Chem. Chem. Phys*, **16**, 22321 (2014).
11. A. K. Opitz, A. Nenning, C. Rameshan, R. Rameshan, R. Blume, M. Hävecker, A. Knop-Gericke, G. Rupprechter, J. Fleig and B. Klötzer, *Angew. Chem. Int. Ed.*, **54**, 2628 (2015).
12. A. K. Opitz and J. Fleig, *Solid State Ionics*, **181**, 684 (2010).
13. A. K. Opitz, M. P. Horlein, T. Huber and J. Fleig, *J. Electrochem. Soc.*, **159**, B502 (2012).
14. Innovative Station for In Situ Spectroscopy: https://www.helmholtz-berlin.de/pubbin/igama_output?modus=einzel&sprache=en&gid=1607&typoid=50740, accessed 2014, Sept. 24th
15. ISISS Station: https://www.helmholtz-berlin.de/pubbin/igama_output?modus=einzel&sprache=en&gid=1671, accessed 2014 Sept. 24th
16. H. Bluhm, M. Hävecker, A. Knop-Gericke, E. Kleimenov, R. Schlögl, D. Teschner, V. I. Bukhtiyarov, D. F. Ogletree and M. Salmeron, *The Journal of Physical Chemistry B*, **108**, 14340 (2004).
17. A. Knop‐Gericke, E. Kleimenov, M. Hävecker, R. Blume, D. Teschner, S. Zafeiratos, R. Schlögl, V. I. Bukhtiyarov, V. V. Kaichev, I. P. Prosvirin, A. I. Nizovskii, H. Bluhm, A. Barinov, P. Dudin and M. Kiskinova, in *Advances in Catalysis*, C. G. Bruce and K. Helmut Editors, p. 213, Academic Press (2009).

18. F. S. Baumann, J. Fleig, H. U. Habermeier and J. Maier, *Solid State Ionics*, **177**, 1071 (2006).
19. S. Kogler, A. Nenning, G. M. Rupp, A. K. Opitz and J. Fleig, *J. Electrochem. Soc.*, **162**, F317 (2015).
20. M. Descostes, F. Mercier, N. Thromat, C. Beaucaire and M. Gautier-Soyer, *Applied Surface Science*, **165**, 288 (2000).
21. D. Neagu, G. Tsekouras, D. N. Miller, H. Ménard and J. T. S. Irvine, *Nat. Chem.*, **5**, 916 (2013).
22. G. Tsekouras, D. Neagu and J. T. S. Irvine, *Energ. Environ. Sci.*, **6**, 256 (2013).